Novel diffraction gratings for next generation Spectrographs with high spectral dispersion

N. Ebizuka*[a], T. Okamoto[a], T. Hosobata[a], Y. Yamagata[a], M. Sasaki[b], M. Uomoto[c], T. Shimatsu[c], S. Sato[d], N. Hashimoto[d], I. Tanaka[e], T. Hattori[e], S. Ozaki[e], W. Aoki[e]

[a]RIKEN, 2-1 Hirosawa, Wako, Saitama, Japan 351-0198, [b]Faculty of Engineering, Toyota Technological Institute, [c]Frontier Research Institute for Interdisciplinary Sciences, Tohoku University, [d]CITIZEN Holdings Co. Ltd., [e]National Astronomical Observatory of Japan

ABSTRACT

As a transmission grating, a surface-relief (SR) grating with sawtooth shaped ridges and volume phase holographic (VPH) grating are widely used for instruments of astronomical observations. However the SR grating is difficult to achieve high diffraction efficiency at high angular dispersion, and the VPH grating has low diffraction efficiency in high diffraction orders. We propose novel gratings that solve these problems. We introduce the hybrid grism which combines a high refractive index prism with a replicated transmission grating, which has sawtooth shaped ridges of an acute apex angle. The birefringence VPH (B-VPH) grating which contains an anisotropic medium, such as a liquid crystal, achieves diffraction efficiency up to 100% at the first diffraction order for natural polarization and for circular polarization. The quasi-Bragg (QB) grating which consists of long rectangular mirrors aligned in parallel precisely, like a window blind, achieves diffraction efficiency of 60% or more in higher than the 4th diffraction order. The volume binary (VB) grating with narrow grooves also achieves diffraction efficiency of 60% or more in higher than the 6th diffraction order. The reflector facet transmission (RFT) grating which is a SR grating with sawtooth shaped ridges of an acute apex angle achieves diffraction efficiency up to 80% in higher than the 4th diffraction order.

Keywords: Echelle, Volume grating, Birefringence grating, Bragg grating, RCWA

1. INTRODUCTION

Diffraction grating for the 8.2m Subaru Telescope [1] and for the next generation huge telescopes of ground-based [2-4] and space-borne [5] are required large angular dispersion and high diffraction efficiency. The physical image size of a star at the focal plane of a ground-based telescope is typically determined by a seeing size. The size of a spectrograph for the ground-based telescope without adaptive optics increases as a size of the telescope increases because a slit width of the spectrograph is proportional to the seeing size, which is proportional to a diameter of the primary mirror of the telescope. Although a space-borne telescope achieves a diffraction-limited imaging, the diameter of the telescope is increased, and light-gathering power increases, astronomers desire a spectrograph with a higher and higher resolving power. Reduction in size and weight of the spectrograph by using a diffraction grating with high angular dispersion is required because restrictions of weight and volume of a scientific instrument for the space-borne telescope are very strict.

In the case of a spectrograph using a reflection grating with the Littrow mount (the configurations which the incident and diffraction angles are equal, and shapes of incident and diffracted beams are identical), since a collimator and camera (imaging optical element) of the spectrograph need to place a large distance from the diffraction grating, the diameters of the collimator and the camera optics become large. On the other hand, a spectrometer using a transmission grating, diameters of collimator and camera optics are able to be smaller than the spectrograph with the reflection grating because the optical elements can place in the close vicinity of the diffraction grating. Moreover, the spectrometer using the transmission grating achieves a long slit spectrum with a small curvature and reduces aberrations for a point image because the spectrograph is able to realize the perfect Littrow mount.

1.1 Surface relief grating

The conventional surface relief (SR) grating with sawtooth shaped ridges (Fig. 1) is commonly used as a transmission grating for a low-dispersion spectrograph and as a grism (the direct diffraction grating). However, in the case of the transmission grating, a diffraction efficiency of an SR grating at the first diffraction order decreases steeply at grating

Advances in Optical and Mechanical Technologies for Telescopes and Instrumentation II,
edited by Ramón Navarro, James H. Burge, Proc. of SPIE Vol. 9912, 99122Z
 · doi: 10.1117/12.2231949

period with 4 times of the wavelength or smaller [6]. Moreover an SR grating of the transmission type is necessary to increase a refractive index of a medium of grating ridges according as a diffraction angle (an angular dispersion) becomes large.

Equations of refractions at incident and exit surfaces of the SR transmission grating in Fig. 1 are given by

$$\sin\theta_0 = \mathrm{n}\sin\theta_1 \tag{1-1}$$

and

$$\mathrm{n}\sin(\alpha-\theta_1) = \sin\theta_2, \tag{1-2}$$

respectively. In the case of the Littrow mount, that is $\theta_2 = \alpha+\theta_0$, the Eq. 1-2 is rewritten as

$$\mathrm{n}\sin(\alpha-\theta_1) = \sin(\alpha+\theta_0)$$

$$\mathrm{n}(\sin\alpha\cos\theta_1 - \sin\theta_1\cos\alpha) = \sin\alpha\cos\theta_0 + \sin\theta_0\cos\alpha$$

$$(\mathrm{n}\cos\theta_1 - \cos\theta_0)\sin\alpha = (\sin\theta_0 + \mathrm{n}\sin\theta_1)\cos\alpha. \tag{1-3}$$

Eq. 1-3 is transformed by substitution of Eq. 1-1 as

$$(\mathrm{n}\cos\theta_1 - \cos\theta_0)\sin\alpha = 2\sin\theta_0\cos\alpha.$$

As the result, the equation for the blazed angle α is given by

$$\tan\alpha = \frac{2\sin\theta_0}{(n\cos\theta_1 - \cos\theta_0)}. \tag{1-4}$$

The Eqs. 1-1, 1-2 and 1-4 apply to the grating ridges with the refractive index of 1.5, the incident and the diffraction angles θ_0 must be smaller than 20° by the restriction of the critical angle for θ_2 which is smaller than 90°. As well as, in the case of θ_0 = 45°, the refractive index of the grating ridges must be larger than 2.3. Clear materials with the refractive index of 2.3 or more in the visible wavelength are limited such as ZnS, ZnSe, TiO_2 and diamond. Especially, no clear material except diamond with the refractive index of 2.3 or more exists in the ultra violet wavelength.

1.2 Volume phase holographic grating

While a volume phase holographic (VPH) grating achieves very high diffraction efficiency up to 100% at the first diffraction order for *S* or *P* polarization [6, 7]. In these reasons, a lot of VPH gratings and VPH grism have been installed in numerous instruments for relatively high-dispersion spectroscopic observations [8-11]. However the VPH grating is not able to achieve high efficiency for natural polarization and circular polarization according as a diffraction angle increases because the properties of the diffraction efficiency are different between *S* and *P* polarization [12]. Moreover, a wavelength bandwidth of a VPH grating is limited by a refractive index modulation of a recoding material using for the VPH grating, which has the maximum of about 0.15 at present [7]. Furthermore, the VPH grating is not suitable for an echelle spectrograph which several to hundreds of diffraction orders are folded onto a two dimensional detector by combination of a grating of high diffraction orders with a cross disperser, such as a prism or a low-dispersion grating of the first diffraction order, because diffraction efficiency of the VPH grating decreases as the diffraction order increases [13].

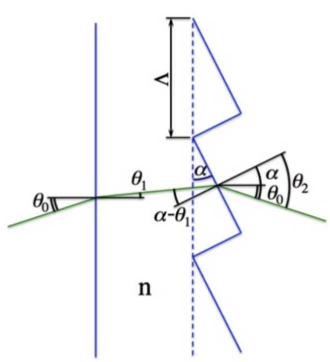

Figure 1 Propagation of incident beam in surface relief grating with saw tooth ridges in the case of the Littrow mount [14].

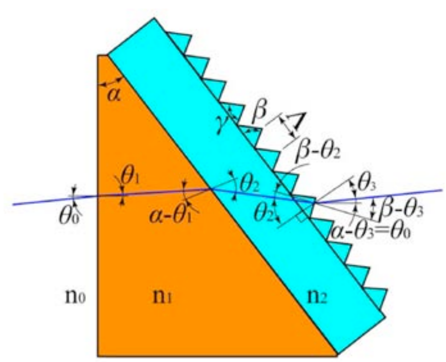

Figure 2 Schematic representation of hybrid grism for MOIRCS.

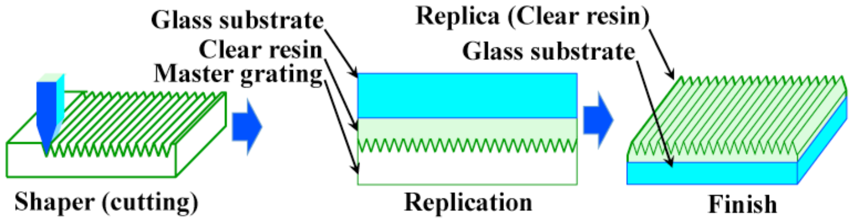

Figure 3 Fabrication process of transmission SR grating with acute angle ridges.

We introduce novel transmission gratings for instruments of the 8.2m Subaru Telescope, the Thirty Meter Telescope (TMT) and the next generation huge telescopes about their expected performances based on simulations and about fabrication methods in this paper [14, 15]. Those are the hybrid grism, the birefringence VPH (B-VPH) grating, the quasi-Bragg (QB) grating, the volume binary (VB) grating and the reflector facet transmission (RFT) grating.

2. HYBRID GRISM

The middle dispersion grisms for the MOIRCS [16] of the Subaru Telescope are fabricated by directly ruling of sawtooth shaped ridges onto a hypotenuse of a KRS-5 (the mixed crystal of TaCl and TaBr) prism. However many cracks like tiny mosaic are seen on the surfaces of the KRS-5 grisms. And the KRS-5 grisms seriously deteriorate efficiency and width of line spectrum. These damages of the grisms are supposed to be caused by repetition of heat cycles between a room temperature and cryogenic temperature when open and shut of the cryostat vessel of the MOIRCS. We have decided the development of hybrid grisms for replacement of the KRS-5 grisms in this reason. The hybrid grism is consisted by the combination of a ZnSe prism (n=2.46@1.65 μm) and replicated SR grating (n~1.5@1.65 μm) with ridges of an acute apex angle.

The beam propagation in the hybrid grism as shown in Fig. 2 is expressed as follows. The equations for refraction at the incident surface of the prism, the boundary between the prism and the glass substrate and the exit surface of a ridge are given by

$$\sin \theta_0 = n_1 \sin \theta_1, \tag{2-1}$$

$$n_1 \sin (\alpha - \theta_1) = n_2 \sin \theta_2 \tag{2-2}$$

and

$$n_2 \sin (\beta - \theta_2) = \sin (\beta - \theta_3), \tag{2-3}$$

respectively. The Eq. 2-3 is transformed by the following procedure as

$$n_2 (\sin \beta \cos \theta_2 - \cos \beta \sin \theta_2) = \sin \beta \cos \theta_3 - \cos \beta \sin \theta_3,$$

$$\tan \beta = \frac{n_2 \sin \theta_2 - \sin \theta_3}{n_2 \cos \theta_2 - \cos \theta_3}. \tag{2-4}$$

The diffraction angle θ_3 is given by equation of diffraction as

$$m\lambda = \Lambda (n_2 \sin \theta_2 - \sin \theta_3). \tag{2-5}$$

$$\sin \theta_3 = n_2 \sin \theta_2 - \frac{m\lambda}{\Lambda}. \tag{2-6}$$

When the diffraction beam is parallel to the incident beam, the blazed angle β is obtained by substitution of $\theta_3 = \alpha - \theta_0$ and the Eq. 2-6 into the Eq. 2-4 as

$$\tan \beta = \frac{m\lambda_0}{\Lambda \left\{ n_2 \cos \theta_2 - \cos (\alpha - \theta_0) \right\}}, \tag{2-7}$$

where λ_0 is the direct vision wavelength. The apex angle γ is given by

$$\gamma = 90 - \beta + \theta_2, \tag{2-8}$$

when θ_2 is parallel to the other facet of the exit surface of the sawtooth shaped ridge.

The hybrid grism for the MOIRCS has the grating period of about 10μm and the apex angle of the sawtooth shaped ridges of about 60°. Figure 3 shows a fabrication procedure of the transmission grating with an acute apex angle for the hybrid grism. The master grating (die) for the hybrid grism is cut onto a surface of a work piece of the nickel-phosphorus alloy, produced by the non-electrolytic plating on a metal substrate, by the shaper process with an ultra-high

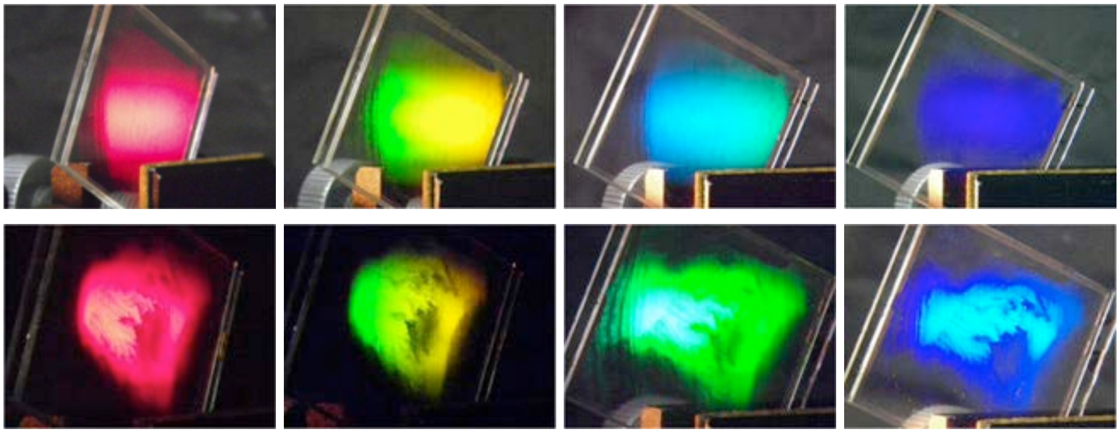

Figure 4 Diffraction image of liquid crystal (LC) gratings of the 1st order. Rows are the same grating, columns are observational (Bragg) angles. Upper row: combination of TKN0100 (UV-curable LC, made by DIC) and MJ041609 (normal LC, made by Merck), UV exposure: 12.4 mW, 180sec. Lower row: combination of ULC17A (UV-curable LC, made by DIC) and MJ041609, UV exposure: 11.0 mW, 180sec.

precision machine and single crystal diamond bit of the same apex angle as the ridge apex angle. The transmission grating with the acute ridge angle is replicated from the master grating. When we had performed a test fabrication of the master grating, we knew that the process is very sensitive to the thermal environment. The isothermal booth for the ultra-high precision machine has improved for temperature stability, and we are performing the second test fabrication.

3. BIREFRINGENCE VPH GRATING

The B-VPH grating consists of an optically anisotropic medium such as a liquid crystal (LC) and optically isotropic medium or consisted with two kinds of optically anisotropic media [17]. We carried out numerical calculations of the diffraction efficiency of the B-VPH gratings by using our own software of the rigorous coupled-wave analysis (RCWA) method [18, 19] that is improved for a diffraction grating with an optical anisotropic medium. We confirmed that the B-VPH grating is able to achieve high diffraction efficiency up to 100 % (neglecting the surface Fresnel's reflection losses) at the first diffraction order with respect to natural polarization and circularly polarization because the characteristics of the diffraction efficiencies of the B-VPH grating is able to coincide *S* and *P* polarizations.

B-VPH gratings which recording materials are combined three kinds of LCs of ultra-violet curable with a normal LC were fabricated by a two beams interferometer with a He-Cd laser (315 nm) as an exposure optical system. The LC gratings have the thickness of the LC layer of 1.3μm and the grating period of 0.45μm. As a result, all of the LC-VPH gratings of combination are able to observe diffraction beams (Fig. 4). However the LC-VPH grating of the combination with LCs of the same maker that is RMC03 (UV-curable LC made by Merck) and MJ041609 (normal LC made by Merck), has week diffraction efficiency. We are going to fabricate LC-VPH gratings with thickness of the LC layer of 10~20μm and the grating period of 1.0μm.

4. QUASI-BRAGG GRATING AND VOLUME BINARY GRATING

The Wide Field Optical Spectrograph (WFOS) which is the first generation instrument of the Thirty Meter Telescope (TMT) is planed to use the reflection gratings in the current design concept [20]. The conventional SR grating of the

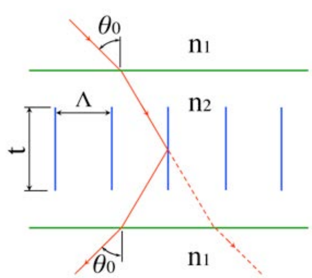

Figure 5 Schematic representation of quasi-Bragg grating.

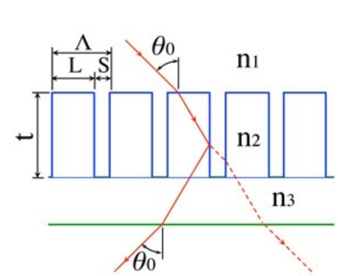

Figure 6 Schematic representation of volume binary grating [14].

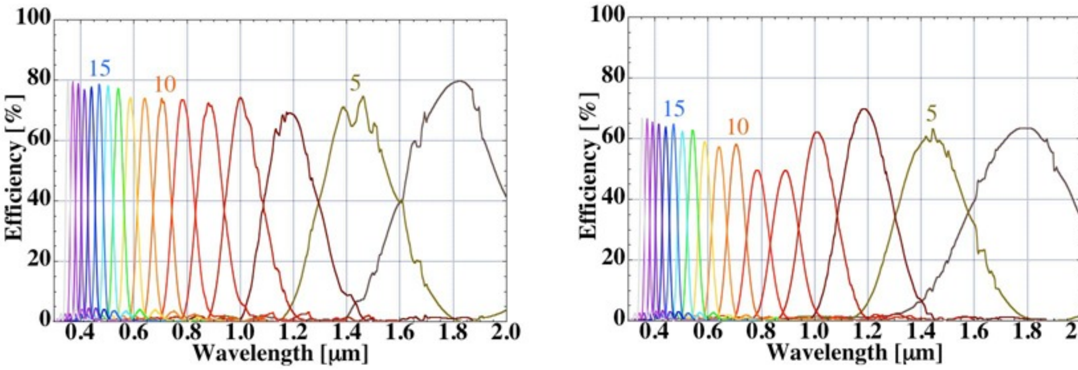

Figure 7 Diffraction efficiencies of QB gratings for the 6th to 20th diffraction orders. n_1 =1.0, n_2 =1.54, Λ = 5 μm, t = 9 μm, θ_0 = 45°. Left panel: *S* polarization, rigtht panel: *P* polarization [14].

reflection type has advantages that the grating achieves comparatively high diffraction efficiency and a grating with a large size is easily fabricated by a replication from a master grating. However a diameter of the camera of the WFOS becomes very large because the Littrow configuration with a reflection grating needs a long distance between the camera and the grating as mentioned in the section of the introduction.

In these reasons, we have evaluated the performance of novel transmission gratings for the WFOS. The transmission gratings have the same incident and diffraction angles of 36~53°, the grating period of 2~5μm, the diffraction orders of 5th~9th and 8th~13rd. However a conventional SR transmission grating and VPH grating are not available for the WFOS gratings as mentioned in the subsection 1.1 and 1.2.

The QB grating [13] which has long rectangular mirrors aligned accurately in parallel like a window blind as shown in Fig. 5 achieves high diffraction efficiencies in higher than the 4th diffraction order at the incident and diffraction angles of 45° as shown in Fig. 7 (neglected surface Fresnel's reflection losses). The dropping of diffraction efficiency of *P* polarization around the 8th and the 9th orders in Fig. 8 is supposed to be influence of the surface plasmon resonance. As well as the VB grating [21, 22] as shown in Fig. 6 achieves high diffraction efficiencies [23] in higher than the 5th diffraction orders at the incident and the diffraction angles of 45° by matching a line and space ratio to coincide *S* polarization with *P* polarization as shown in Fig. 8 (including the reflection loss by the incident surface). It is able to regard the VB grating as a QB grating in this case because grooves of the VB grating function as total reflection mirrors. The droppings of diffraction efficiency of *S* polarization below the 6th order and of *P* polarization below the 4th order in Fig. 9 are supposed to be influence of the evanescent wave coupling between a ridge and the next ridge beyond the groove. And the reason of *P* polarization achieves higher efficiency than *S* polarization in Fig. 9 is suppose to be that the incident angle is close to the Brewster angle.

4.1 Fabrications of quasi-Bragg grating

The first fabrication of the QB grating was done by stacking of 40 sheets of quartz mirror substrates. The mirror substrate is a thickness of 0.2 mm, and chromium as a mirror is deposited on one side. The mirror substrates were laminated by an optical adhesive mixed with glass beads of 10 μm in diameter. However, the QB grating did not function as a diffraction grating in the visible wavelength because the glass beads have large variations in diameter [14, 15].

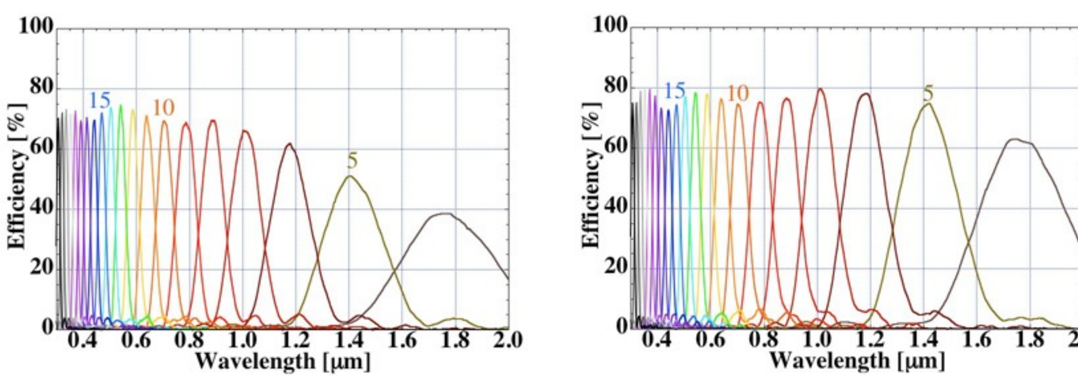

Figure 8 Diffraction efficiencies of VB gratings for the 6th to 24th diffraction orders. n_1 =1.0, n_2 =1.54, Λ = 5 μm, L&S = 4.75:0.25 [μm], t = 9 μm, θ_0 = 45°. Left panel: *S* polarization, right panel: *P* polarization [14].

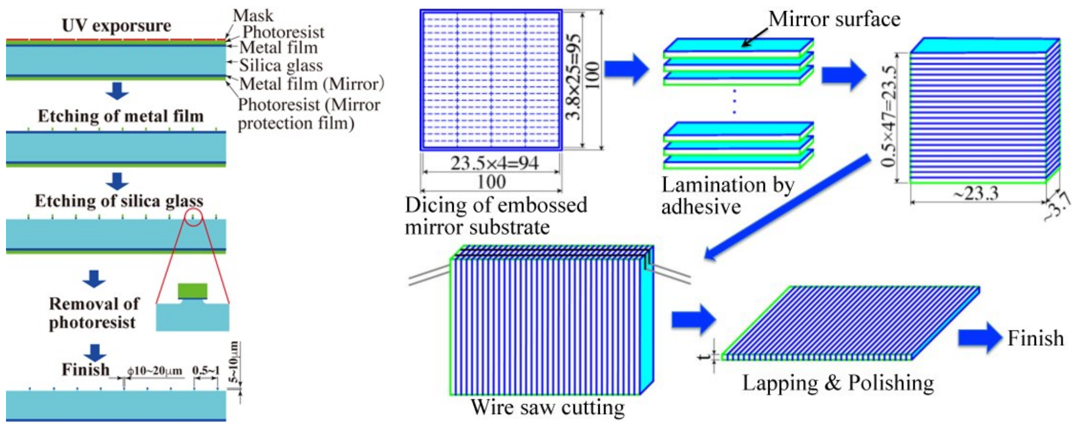

Figure 9 Schematic representation of fabrication method of quasi-Bragg grating.

The subsequent fabrications of the QB grating of 20 sheets of quartz mirror substrates with a thickness of 0.5 mm and with a uniform gold film deposited onto both sides were laminated by atoms fusion bonding at room temperature in air, processed by the Frontier Research Institute for Interdisciplinary Sciences, Tohoku University [24]. The QB grating has very high accuracy as regarding the grating period, which is available for the visible wavelength, because a symmetrical diffraction pattern was seen [14].

The third fabrications of the QB grating were lamination of 47 sheets of mirror substrates of quartz glass with a thickness of 0.5 mm as shown in Fig. 9. The substrate has a chromium mirror deposited onto one surface, and the back surface of the mirror substrate was embossed by wet etching itself, as maintaining thickness of the substrate as shown in left panel of Fig. 9. The etching was processed by the Nanotechnology Platform facilities of the Toyota Technology Institute. The mirror substrates were laminated by a UV-curable optical adhesive as shown in right panel of Fig. 9. Although the QB grating did not show optimal condition of adhesion as it has partial periodic errors, the lattice spacing of the grating achieves practical accuracy even in visible light [14].

4.2 Fabrications of Volume binary grating

To achieve a thick binary grating with a high aspect ratio, we are developing a fabrication method for the thick binary grating by applying MEMS (Micro Electro Mechanical Systems) technology in the Nanotechnology Platform facilities. We had fabricated volume binary gratings of a photoresist, which grating period is 5 μm, line and space ratio is 4:1 and thickness of the grating is 10 μm. However a uniform VB grating with a large area was hard to fabricate by this process.

We are planning to develop a high-dispersion echelle grism for MOIRCS which grating period is 5.1 μm, line and space ratio is 9:1, thickness of the grating is 16 μm and Bragg angle in the vacuum is 28.4°. The master grating for the grism is going to fabricate by the Bosch process as shown in Fig.10.

5. REFLECTOR FACET TRANSMISSION GRATING

The RFT grating is an SR grating with saw-tooth shaped ridges of an acute apex angle as shown in Fig. 11. The incident beam from one side of a ridge of the RFT grating is reflected by another surface of the ridge, and the diffraction beam is exited from the rear surface of the RFT grating. In order to increase a diffraction angle, a refractive index of the conventional SR transmission grating has to increase because the beam in the SR grating is folded by refraction at the incident

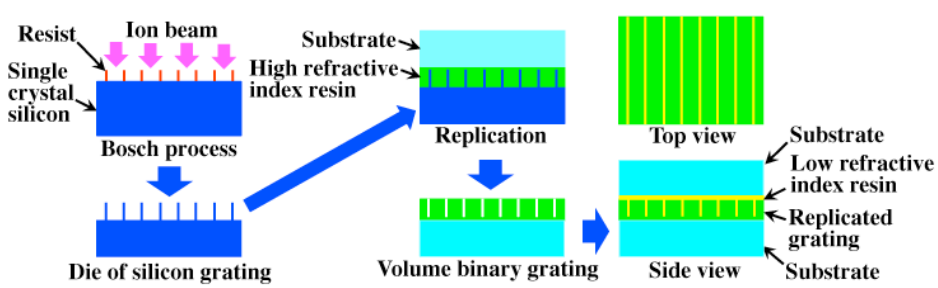

Figure 10 Schematic representation of fabrication method for VB grating.

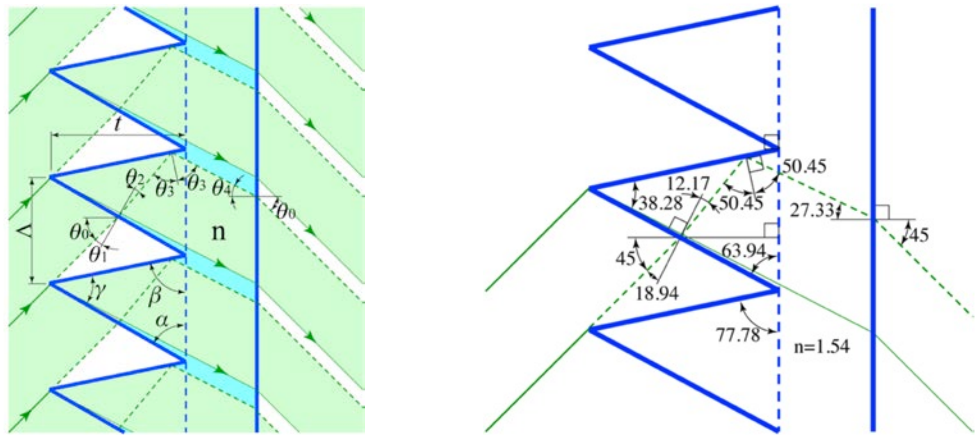

Figure 11 Schematic representation of beam propagation in reflector facet transmission (RFT) grating (Left panel). Refraction and reflection angles of beam in RFT grating when incident and exit angle of beam are 45° (Right panel).

and the exit interfaces, as mentioned in the subsection 1.1. On the other hand, the RFT grating is able to use a large diffraction angle even with a small refractive index of the grating ridges because the beam is folded by reflection in the RFT grating.

5.1 Basic equations for reflector facet transmission grating

The beam propagation in the RFT grating as shown in the left panel of Fig. 11 is expressed as follows. The equations for an incident angle θ_1 and refraction angle θ_2 at the incident surface of the ridge are given by

$$\theta_1 = \alpha\text{-}\theta_0 \tag{5-1}$$

and

$$\sin\theta_1 = n \sin\theta_2, \tag{5-2}$$

respectively. The relations in θ_2, reflection angle θ_3 at the other surface of the ridge and the apex angle γ of the ridge is obtained by the sum of the interior angles of the triangle as

$$\mathrm{R}+\theta_2+\mathrm{R}-\theta_3+\gamma = 2\mathrm{R},$$

$$\theta_3 = \theta_2+\gamma. \tag{5-3}$$

As well as the relation in θ_3, the reflected beam angle θ_4 at the exit surface and the angle of the refraction surface β is obtained by

$$\theta_3+\theta_4+2\mathrm{R}-\beta = 2\mathrm{R},$$

$$\theta_4 = \beta\text{-}\theta_3. \tag{5-4}$$

The equation for refraction at the exit surface of the RFT grating is given by

$$n \sin\theta_4 = \sin\theta_0. \tag{5-5}$$

When the reflected beam propagates parallel from an angle ϕ to the incident surface, the angle of the incident surface α is obtained by

$$\theta_4 = \mathrm{R}-\alpha+\phi,$$

$$\alpha = \mathrm{R}-\theta_4+\phi. \tag{5-6}$$

Eq. 5-3 is transformed by substitution of Eq. 5-4 and the sum of the interior angles of a triangle: $\gamma + \alpha + \beta = 2\mathrm{R}$ as

$$\theta_2 = \alpha+2\beta-\theta_4-2\mathrm{R}. \tag{5-7}$$

The angle of reflector surface β is obtained by transformation of Eq. 5-7 as

$$\beta = (\theta_2+\theta_4-\alpha)/2+\mathrm{R}. \tag{5-8}$$

Note that the RFT grating does not achieve its essential performance if a beam enters from back surface of the ridges because a part of the beam is folded to irregular direction by the ridges.

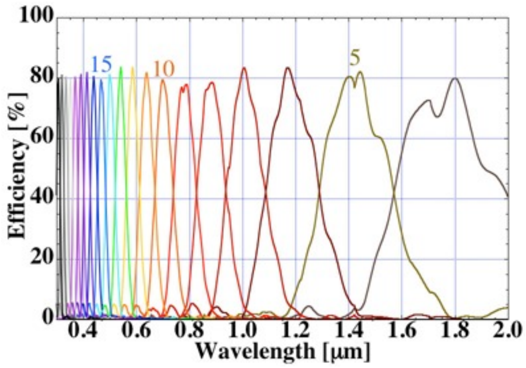

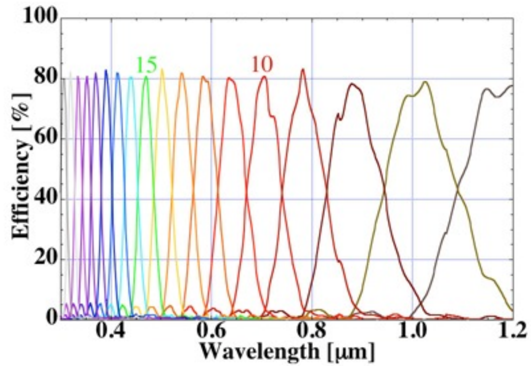

Figure 12 Diffraction efficiencies of RFT gratings for the 6th to 24th diffraction orders. n_0 =1.0, n_1 =1.54, Λ = 5 μm, t = 9 μm, θ_B = 45°. Left panel: *S* polarization, right panel: *P* polarization.

5.2 Example of caluclation of RFT grating

The inverse ray tracing of the RFT grating is expressed as follows, when a incident and exit angle of beam for a RFT grating are 45°, the refractive index of ridges of the RFT grating is 1.54 as shown in the right panel of Fig. 11. The angle of θ_4 is obtained by substitution of θ_0 = 45° and n =1.54 in Eq. 5-5 as

$$\theta_4 = \sin^{-1}\left(\frac{\sin 45°}{1.54}\right)$$

$$= 27.33°.$$

When the diffraction angle in the vacuum is 45°±2.5°, the angle ϕ is obtained by

$$\phi = \sin^{-1}\left\{\frac{\sin(45° + 2.5°)}{1.54}\right\} - \theta_4$$

$$= 1.27°.$$

The angle of incident surface α is obtained by substitution of the values of θ_4 and ϕ in Eq. 5-6 as

$$\alpha = 90°\text{-}27.33\text{+}1.27°$$

$$= 63.94°.$$

The angle of reflector surface β is obtained by substitution of α, θ_0, n and θ_4 in Eq. 5-8 as

$$\beta = \frac{1}{2}\left[\sin^{-1}\left\{\frac{\sin(63.94° - 45°)}{1.54}\right\} + 27.33° - 63.94°\right] + 90°$$

$$= 77.78°.$$

The angles γ, θ_3, θ_2 and θ_1 are obtaind by the sum of the interior angles of the triangle, Eqs 5-4, 5-3 and 5-2 as

$$\gamma = 2R\text{-}\alpha - \beta = 180°\text{-}63.94°\text{-}77.78°$$

$$= 38.28°.$$

$$\theta_3 = \beta\text{-}\theta_4 = 77.78°\text{-}27.33°$$

$$= 50.45°,$$

$$\theta_2 = \theta_3\text{-}\gamma = 50.45°\text{-}38.28°$$

$$= 12.17°$$

and

$$\theta_1 = \sin^{-1}(n \sin\theta_2) = \sin^{-1}(1.54 \times \sin 12.17°)$$

$$= 18.94°,$$

respectively. The angle θ_1 is also obtaind by Eq. 5-1 as

$$\theta_1 = \alpha - \theta_0 = 63.94° - 45°$$
$$= 18.94°.$$

We are planning to fabricate a master grating of a RFT grating by using the same method as the fabrication process of the hybrid grism (Fig. 3).

6. CONCLUSIONS

In this paper, we introduced innovative diffraction gratings. The hybrid grism is consisted by combination of a ZnSe prism and replicated surface-relief grating with ridges of an acute apex angle. The B-VPH grating is able to achieve high diffraction efficiency of up to 100% for the natural polarization and the circular polarization at the first diffraction order. The QB grating and the VB grating achieve comparative high diffraction efficiency in high diffraction orders. The RFT grating is able to use for a large diffraction angle. The RFT grating achieves high diffraction efficiency of up to 80% in high diffraction orders. These types of diffraction gratings are useful for new instruments on both the existing 8m class of telescopes, as well as the upcoming 30m class and the space-borne telescopes, due to their ability to produce high spectral dispersion from a relatively small pupil, thereby making the whole instrument smaller, more practical, and less expensive.

We appreciate Ken Kajiwara and Toshio Okumura of Nanotechnology Platform facilities, the Toyota Institute of Technology for their assistance on the trial fabrications of the VB gratings. We thank Masahiro Takeda of RIKEN for his assistance on the trial fabrications of master gratings for the hybrid grism and the RFT grating. The first prototype of QB gratings was fabricated by KOGAKU GIKEN Corp. The second and third prototypes of the QB gratings were partially fabricated by Crystal Optics Co. Ltd. We utilize facility of the Advanced Technology Center of National Astronomical Observatory of Japan (NAOJ) for grating measurements and "Nanotechnology Platform Japan" of the Ministry of Education, Culture, Sports, Science and Technology (MEXT), Japan. This work is supported by the grant-in-aid of NAOJ for TMT strategic basic research and development, by the Grant-in-Aid for Challenging Exploratory Research, 2015-2016, 15K13470; from MEXT. And this work was supported by the grant-in-aid of NAOJ for Joint development research, and by Adaptable and Seamless Technology Transfer Program through Target-driven R&D from Japan Science and Technology Agency.

REFERENCES

[1] N. Takato and I. Iwata, "Instrumentation at the Subaru Telescope," Proc. SPIE **8446**, 8446051-0510 (2012).
[2] L. Simard, et al., "The instrumentation program for the Thirty Meter Telescope," Proc. SPIE **8446**, 84461F1-1F10 (2012).
[3] Jacoby, G. H., et al., "The instrument development and selection process for the Giant Magellan Telescope," Proc. SPIE **8446**, 84461G1-1G16 (2012).
[4] Casali, M. M., Pasquini, L. and Ramsay, S., "Overview of the ESO instrumentation program," Proc. SPIE **8446**, 8446041-047 (2012).
[5] T. Nakagawa, et. al., "The next-generation infrared astronomy mission SPICA under the new framework," Proc. SPIE **9143**, 91431I1-1I9 (2014).
[6] Oka, K., et al., "Optimization of a volume phase holographic grism for astronomical observation using the Photopolymer," Proc. SPIE **5005**, 8-19 (2003).
[7] Barden, S.C., Arns, J.A. and Colburn, W.S., "Volume-phase holographic gratings and their potential for astronomical applications," Proc. SPIE **3355**, 866-876 (1998).
[8] Uehara, M., *et al*., "Development of the Wide Field Grism Spectrograph 2," Proc. SPIE **5492**, 661-668 (2004).
[9] Watanabe, M., *et al*., "TRISPEC: A Simultaneous Optical and Near-Infrared Imager, Spectrograph, and Polarimeter," PASP **117**, 870-884 (2005).
[10] Ebizuka, N., et al., "Cryogenic VPH Grisms for MOIRCS," PASJ **63**, S605-S612 (2011).
[11] Ebizuka, N., et al., "Grisms Developed for FOCAS," PASJ **63,** S613-S622 (2011).
[12] Baldry, I. K., Bland-Hawthorn, J. and Robertson, J. G., "Volume Phase Holographic gratings: Polarization properties and Diffraction Efficiency," PASP **116,** 403-414 (2004).

[13] Oka, K., Ebizuka, N. and Kodate, K., “Optimal design of the grating with reflective plate of comb type for astronomical observation using RCWA,” Proc. SPIE **5290**, 168-178 (2004).

[14] Ebizuka, N., *et al.*, “Diffraction Gratings for the Latest Visible and Infrared Astronomical Observations,” Publ. Jpn. Soc. Infrared **26**, in press (2017).

[15] Ebizuka, N., et al., "Birefringence Bragg Binary (3B) Grating, Quasi-Bragg Grating and Immersion Gratings," Proc. SPIE **9151**, 91515C1-5C9, (2014).

[16] Ichikawa, T., “MOIRCS: multi-object infrared camera and spectrograph for SUBARU,” Proc. SPIE **6269**, 626916 (2006).

[17] Montemezzani, G. and Zgonik, M., “Light diffraction at mixed phase and absorption gratings in anisotropic media for arbitrary geometries,” Phys.Rev. **E 55**, 1035-1047 (1997).

[18] Moharam, M. G. and Gaylord, T. K., “Rigorous coupled-wave analysis of planar-grating diffraction,” JOSA **71**, 811 (1981).

[19] Li, L., “Note on the S-matrix propagation algorithm,” JOSA **A 20**, 655 (2003).

[20] Pazder, J. S., et al., “WFOS: a wide field optical spectrograph for the Thirty Meter Telescope,” Proc. SPIE **6269**, 62691X (2006).

[21] Gupta, M. C. and Peng, S. T., “Diffraction characteristics of surface-relief gratings,” Appl. Opt. **32**, 2911-2917 (1993).

[22] Gerritsen, H. J. and Jepsen, M. L., “Rectangular surface-relief transmission gratings with a very large first- order diffraction efficiency (95%) for unpolarized light,” Appl. Opt. **37**, 5823-5829 (1998).

[23] Bianco, A. and Ebizuka, N., “Echelle VPHG: a step forward,” Proc. SPIE **8450**, 431-438 (2012).

[24] Shimatsu, T. and Uomoto, M., “Room Temperature Bonding of Wafers with Thin Nanocrystalline Metal Films,” ECS Transactions **33**, 61-72 (2010).

第41回光学シンポジウム

講演番号 22

次世代天文学観測装置用の新しい高分散回折格子 II

Novel Gratings with high angular dispersion for Next Generation Instruments of Astronomical Observations II

○海老塚 昇[1), 岡本 隆之[1), 細畠 拓也[1), 山形 豊[1), 佐々木 実[2), 魚本 幸[3), 島津 武仁[3), 佐藤 慎也[4), 橋本 信幸[4), 森田 晋也[5), 田中 壱[6), 服部 尭[6), 尾崎 忍夫[6), 青木 和光[6)

○N. Ebizuka[1), T. Okamoto[1), Y. Yamagata[1), M. Sasaki[2), M. Uomoto[3), T. Shimatsu[3), S. Sato[4), N. Hashimoto[4), S. Morita[5), I. Tanaka[6), T. Hattori[6), S. Ozaki[6), W. Aoki[6)

理化学研究所 [1),豊田工業大学 工学部 [2), 東北大学 学際科学フロンティア研究所 [3), シチズンホールディングス（株）開発部 [4), 東京電機大学 工学部 [5), 国立天文台 [6)

RIKEN[1), Faculty of Engineering, Toyota Technological Institute[2), Frontier Research Institute for Interdisciplinary Sciences, Tohoku University[3), CITIZEN Holdings Co. Ltd.[4), Faculty of Engineering, Tokyo Denki University[5), National Astronomical Observatory of Japan[6)

As a transmission grating, a surface-relief (SR) grating with sawtooth shape grooves and volume phase holographic (VPH) grating are widely used for instruments of astronomical observations. However the SR grating and the VPH grating are difficult to achieve high diffraction efficiency at high angular dispersion. We propose two novel gratings that solve this problem. One is the birefringence VPH grating, which contains anisotropic media such as liquid crystals. The other is the quasi-Bragg (QB) grating, which consists long rectangle thin metallic films or low refractive index layers aligned in parallel precisely such as a window shade. We also introduce the hybrid grism, which combines a high refractive index prism and replicated transmission grating with sawtooth shape grooves of acute angle.

１．はじめに

天体望遠鏡の大型化にともなって集光力が増大し、測定精度が格段に向上するとともに、分光観測装置の適用範囲は広がっている。たとえば、近年、急速な進展をみせている太陽系外惑星の探査・研究においては、高分散分光器を用いた中心星の視線速度変化の観測から地球質量の惑星の検出や、惑星大気を透過する中心星の光の分光観測によって惑星大気の成分を分析することが可能になってきている。しかし、地上における分光観測装置は、補償光学を使用しない場合には大気揺らぎによって天空上での星像サイズ（典型的には 1 秒角程度）が決まってしまうため、望遠鏡の口径が大きくなると焦点上の星像サイズも大きくなってしまう。この星像にあわせたスリット幅で分光観測を行うと、同じ波長分解能を達成するためには分光観測装置を望遠鏡の口径に比例（体積では口径の 3 乗に比例）して大きくしなければならない。

宇宙望遠鏡の場合、回折限界の観測を達成できるので、望遠鏡の口径が変わっても、波長と分解能等の性能が同じ分光観測装置のサイズは変わらない。しかし、大気圏外における観測装置は重量や体積に対する制限が極めて厳しい。その結果、次世代大型望遠鏡用の分散光学素子には、観測装置の小型・軽量化のために、大きな角分散と高い効率が求められる。

8.2m すばる望遠鏡 [1)や国内外の中小口径望遠鏡の観測装置用に様々な表面刻線型（SR: Surface Relief）グリズム（直視回折格子）や Volume phase holographic (VPH) グリズムが開発されている [2-6)。しかし、格子が鋸歯形状の透過型の SR grating は 1 次回折光に対して格子周期が波長の 4 倍以下になると回折効率が急激に低下してしまう [7)。一方、VPH grating は格子周期が波長の 0.7~4 倍において、1 次回折光の S あるいは P 偏光に対して最大 100%の回折効率を達成することができる [7, 8)。しかし、VPH grating は S と P 偏光に対する回折効率の特性が異なるために、ブラッグ角（角度分散）が大きくなるのに従って S と P 偏光の回折効率の差異が大きくなり、自然偏光や円偏光に対して高い回折効率を達成できなくなる [9)。また、VPH grating に利用される記録材料は屈折率の変調量が現状では最大 0.15 程度であり、波長帯域幅が屈折率の変調量に比例するためにその制限を受けてしまう。さらに VPH grating は 2 次以上の高次回折光において高い回折効率を達成することができなくなるために、高次回折光を利用するエシェル分光器には使用できない [8, 10)。

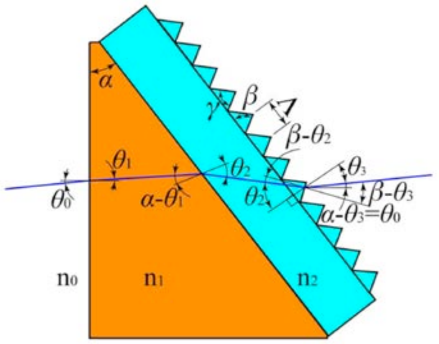

Fig.1 Schematic representation of hybrid grism for MOIRCS.

本講演において 8.2m すばる望遠鏡の MOIRCS（近赤外線多天体分光撮像観測装置）[11]用に開発を行っている高屈折率プリズムとレプリカの SR grating を組み合わせたハイブリッド-グリズムや、30m クラス次世代巨大地上望遠鏡 [12] および 2.5~10m クラスの次世代大型宇宙望遠鏡 [13] の観測装置用の新しい分散光学素子として実用化を目指している Birefringence VPH grating や Quasi-Bragg (QB) grating 等の特徴および性能について紹介する [10, 14-17]。

2. バイブリッド-グリズム

MOIRCS 用の中分散グリズムは KRS-5（塩化タリウムと臭化タリウムの混晶）のプリズムにルーリングエンジンによって鋸歯形状の溝を直接加工されたものである。しかし、このグリズムは装置の開閉の度に常温と 100K の温度サイクルが繰り返された結果、表面に細かい亀裂が入り、効率が著しく低下してしまった。

そこで Fig. 1 のように ZnSe プリズム（n=2.5）にレプリカ（n=1.5）の SR 回折格子を組合せたバイブリッド-グリズムを開発することになった。

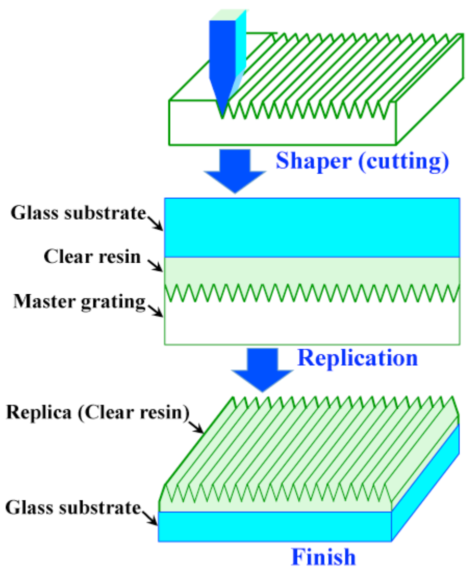

Fig.2 Fabrication process of transmission SR grating with acute angle grooves.

このバイブリッド-グリズムは格子間隔が約 10μm、格子の頂角が 60°程度の鋭角になる。この表面刻線型回折格子の製作方法を Fig. 2 に示す。まず、刃先を格子形状と同じ角度の単結晶ダイアモンドバイトを超精密加工装置に取り付けて無電解メッキのニッケル・リン合金のワークピースをシェーパー加工によって金型が製作される。金型に離型材を塗布して紫外線硬化型等の樹脂を滴下した後に平行平面基板を置き、基板側から紫外線露光を行ない、金型を剥離することによって完成する。シェーパー加工の条件出しを行った結果、この加工は加工機の温度環境に極めて敏感であることがわかり、現在は恒温ブースの温度を安定させるための改造を行っている。

3. Birefringence VPH grating

透過型の VPH grating において，ホログラム記録材料として液晶等の光学異方性媒質と等方生媒質、あるいは 2 種類の光学異方性媒質を組み合わせた場合に、任意のブラッグ角において光学異方性媒質と等方生媒質の屈折率を調整して、偏光と P 偏光の 1 次回折光の回折効率特性を一致させることによって、自然偏光や円偏光に対しても高い回折効率を達成できるようになる [14, 15, 17]。我々が独自に作成した厳密結合波解析

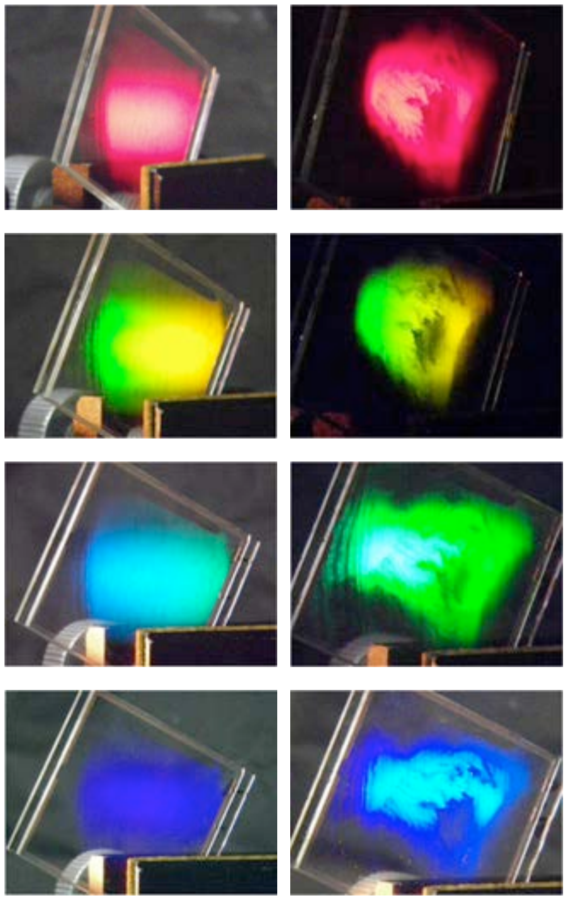

Fig. 3 Diffraction image of liquid crystal gratings with the 1st order. Rows are the same grating, columns are different observation (Bragg) angles.

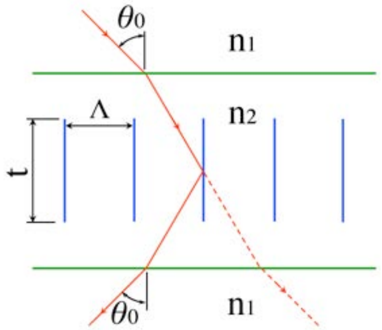

Fig.4 Schematic representation of quasi-Bragg grating.

（RCWA）[18, 19]のソフトウエアを光学異方性媒質にも対応できるように改良して、Birefringence VPH grating が自然偏光や円偏光に対して最大100%の回折効率を達成できることを確認した[16)]。

我々は 3 種類の紫外線硬化型の液晶をそれぞれ通常の液晶（1 種類）と混合して、紫外線レーザの二光束干渉計を用いた干渉露光によって Birefringence VPH grating の試作を行った。その結果、いずれの組み合わせでも回折光を観察することができた（Fig. 3）。

4. Quasi-Bragg grating

鋸歯形状の格子の SR grating は入射角と回折角が大きくなると、格子と空気の界面の臨界角によって回折光を回折格子から取り出せなくなる。これを避けるためには格子の媒質の屈折率を高くしなければならない[16, 17)]。前述のように VPH grating は次数が高くなると回折効率が低下してしまう。一方、高屈折率のプリズムに階段形状の回折格子を可視光波長域において精度よく一体加工することは困難である。

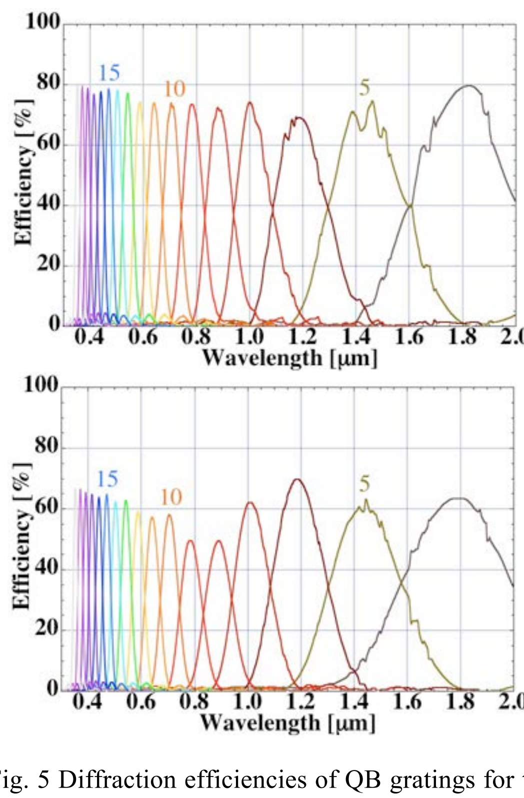

Fig. 5 Diffraction efficiencies of QB gratings for the 6th to 20th diffraction orders. n_0 =1.0, n_1 =1.54, Λ = 5 μm, t = 9 μm, θ_B = 45°. Upper panel: S polarization, Lower panel: P polarization[17)].

Fig. 4 のように短冊状の金属膜あるいは低屈折率層が鎧戸やブラインドのように精度よく平行に配列された Quasi-Bragg (QB) grating[10, 20)] は高次回折光において高い回折効率を達成できることが RCWA 法の数値解析によって確認されている（Fig.5）[10, 17)]。

東北大学 学際科学フロンティア研究所において、両面に厚さが均等な金の膜を堆積させた厚さ 0.5mm の石英ミラー基板 20 枚を常温接合法[21)]により積層して QB grating を試作した。また、平行平面基板自体をエッチングして厚さを維持したスペーサを形成した基板を積層することによって、格子周期の精度が高い QB grating を実現する方法を考案した。Fig. 6 のようにクロムがスパッタリングされたミラー面の裏面にエッチングによりエンボス（スペーサ）を形成した 0.5mm の石英ミラー基板 47 枚を紫外線硬化型接着剤により積層して、QB grating を試作した。

これらの QB grating と以前に試作したクロムがスパッタリングされたミラー基板をガラスビーズが混入された接着剤で積層した QB gratin の回折像を観察したところ、ガラスビーズが混入された接着剤で積層した QB gratin は、ガラスビーズの直径のばらつきのために、Fig. 7 の上段のように可視光においては回折格子として機能しないことがわかった。一方、常温接合法により積層された QB grating は Fig. 7 の中段のように可視光において極めて高い格子周期精度であることが分かった。また、エンボス基板を積層した QB grating は接着の条件が最適ではなかったため、Fig. 7 の下段のように部分的に周期誤差

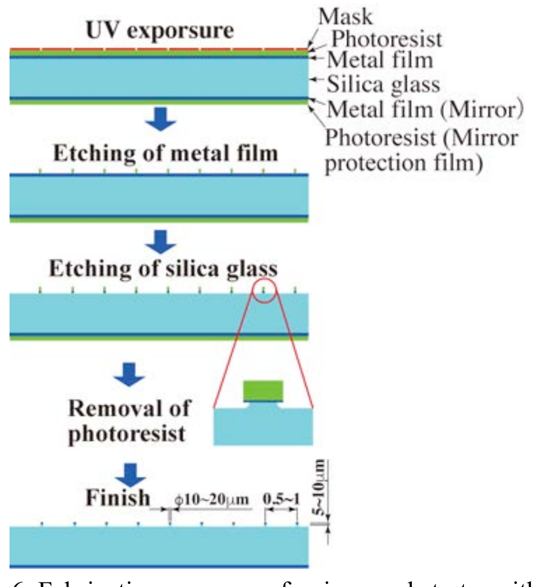

Fig.6 Fabrication process of mirror substrate with emboss for QB grating.

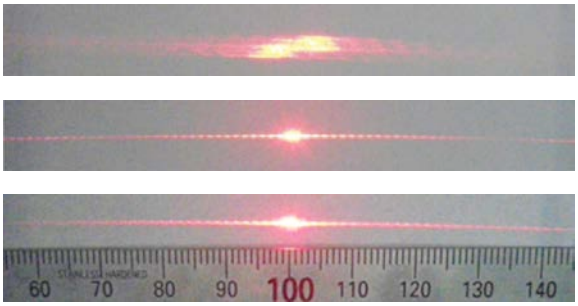

Fig. 7 Diffracted beam images of QB gratings, Quasi-Bragg angle: 45°. QB grating on the top panel shows that silica glass substrates of 0.2mm in thickness deposited with a chromium film on one side are laminated by adhesive mixed with glass beads of 10 μm in diameter. QB grating on the middle panels shows that silica glass substrates of 0.5 mm in thickness deposited with gold film on both sides are laminated by fusion of gold at room temperature[21)]. QB grating on the bottom panels shows that silica glass substrates of 0.5 mm in thickness with emboss laminated by adhesive[17)].

があるものの、可視光においても実用的な精度の格子間隔を実現できることを確認した。

5. おわりに

本稿で紹介したハイブリッド-グリズムは高屈折率のプリズムに溝を直接加工したグリズム（ソリッド-グリズム）と比べて、高い回折効率を達成できる上、開発期間を短くできると期待されている。また、Birefringence VPH grating は入射角と回折角（ブラッグ角）が真空中において 30°を超える場合であっても自然偏光や円偏光に対して 1 次回折光の回折効率が最大 100%を達成できる。一方、QB grating は高次回折光において高い効率を達成することができる。我々はミラー基板の常温接合やエンボス付きミラー基板の積層により、高精度な QB grating が製作できることを示した。

豊田工業大学のナノテクノロジープラットフォーム技術支援員の梶原 健氏と奥村 俊雄氏には素早い対応をしていただき、短期間に劇的な技術革新と微細な深い矩形格子に対する多くの知見が得られた。本研究の回折格子や光学部品等の試作や測定は主に国立天文台先端技術センターの設備を利用させていただいている。本研究は日本科学技術振興機構の A-Step 探索タイプ予算および、科学研究費 挑戦的萌芽研究、国立天文台共同開発研究経費、TMT 戦略的基礎開発研究経費の支援により推進された。

文献

1) N. Takato and I. Iwata: *Proc. SPIE,* **8446** (2012) 05-1.
2) M. Uehara *et al*.: *Proc. SPIE*, **5492** (2004) 661.
3) M. Watanabe *et al*.: *Publ. Astron. Soc. Pacific*, **117** (2005) 870.
4) 海老塚 昇: 光学, **39** (2010) 566.
5) N. Ebizuka *et al.*: *Publ. Astron. Soc. Jpn.,* **63** (2011) S605.
6) N. Ebizuka *et al.*: *Publ. Astron. Soc. Jpn.,* **63** (2011) S613.
7) K. Oka, N. Ebizuka and K. Kodate: *Proc. SPIE,* **5005** (2003) 8.
8) S. C. Barden *et al.*: *Publ. Astron. Soc. Pacific,* **112** (1998) 809.
9) I. K. Baldry, J. Bland-Hawthorn and J. G. Robertson: Publ. *Astron. Soc. Pacific,* **116** (2004) 403.
10) K. Oka, N. Ebizuka and K. Kodate: *Proc. SPIE,* **5290** (2004) 168.
11) T. Ichikawa et al.: *Proc. SPIE,* **6269** (2006) 38.
12) L. Simard *et al.*: *Proc. SPIE,* **8446** (2012) 1F-1.
13) T. Nakagawa *et al.*: *Proc. SPIE,* **9143** (2014) 1I-1.
14) 海老塚 昇, 他: 光学シンポジウム, **37** (2012) 12.
15) N. Ebizuka *et al.*: *Proc. SPIE,* **9151** (2014) 5C1.
16) 海老塚 昇, 他: 光学シンポジウム, **40** (2015) 20.
17) N. Ebizuka *et al.*: 日本赤外線学会誌, (2016) in press.
18) M. G. Moharam, and T. K. Gaylord: JOSA, **71** (1981) 811.
19) L. Li: J. Opt. Soc. Am., **A 20** (2003) 655.
20) 岡 恵子, 海老塚 昇, 小舘 香椎子: 光学シンポジウム, **29** (2004) 85.
21) T. Shimatsu and M. Uomoto: ECS *Trans.*, **33** (2010) 61.